Photoacoustics 9 (2018) 31–38

Contents lists available at ScienceDirect

Photoacoustics

journal homepage: www.elsevier.com/locate/pacs

Continuous wave laser diodes enable fast optoacoustic imaging

Antonios Stylogiannis[a,1], Ludwig Prade[a,1], Andreas Buehler[a], Juan Aguirre[a], George Sergiadis[a,b], Vasilis Ntziachristos[a,*]

[a] Institute of Biological and Medical Imaging, Technische Universität München, Munich, Germany and Helmholtz Zentrum München, Neuherberg, Germany
[b] Department for Electrical and Computer Engineering, Aristotle University, 54124 Thessaloniki, Greece

ARTICLE INFO

Article history:
Received 24 July 2017
Received in revised form 22 November 2017
Accepted 14 December 2017
Available online 16 December 2017

Keywords:
Photoacoustic
Light sources
Light-emitting diodes
Current drivers
Visible
Near-infrared

ABSTRACT

Pulsed laser diodes may offer a smaller, less expensive alternative to conventional optoacoustic laser sources; however they do not provide pulse rates faster than a few tens of kHz and emit at wavelengths only within the near-infrared region. We investigated whether continuous wave (CW) laser diodes, which are available in visible and near-infrared regions, can be good optoacoustic light sources when overdriven with a peak current >40-fold higher than the CW absolute maximum. We found that overdriven CW diodes provided ~10 ns pulses of ~200 nJ/pulse and repetition rates higher than 600 kHz without being damaged, outperforming many pulsed laser diodes. Using this system, we obtained images of phantoms and mouse ear and human arm *in vivo*, confirming their use in optoacoustic imaging and sensing.

1. Introduction

Optoacoustic measurements are typically performed by employing light pulses in the nanosecond pulse-width range. Ultra-short pulses are important for satisfying stress and thermal confinement requirements and for maximizing the signal-to-noise ratio (SNR) and the imaging resolution achieved [1–6]. Fast pulsing rates are also important as they can accelerate raster-scan times in imaging applications and possibly further improve the SNR through signal averaging. An additional critical parameter of optoacoustic illumination is the energy per pulse delivered to tissue. Clinical and small animal optoacoustic systems considered for macroscopic imaging at depths of several millimeters to centimeters require nanosecond pulses of 10–100 mJ/pulse [7]. Such energies are typically delivered by expensive, slow and technologically complex lasers, such as Q-switched Nd:YAG or dye lasers, which attain large form factors and can require forced cooling and frequent realignment. Optical parametric oscillators (OPOs) or different dyes impart the ability to generate different wavelengths, but this further increases cost and complexity of the illumination source.

Compared to macroscopic imaging, optoacoustic microscopy and mesoscopy typically operate at depths in the micrometer and millimeter range [8], respectively. Several microscopy or mesoscopy implementations have been based on pulsed-OPO or dye laser technology [9], typically using more cost-effective laser versions compared to macroscopy, due to the lower energy-per-pulse requirements. Nevertheless, pulsed OPO and dye laser technologies are not appropriate for miniaturization or drastic cost reduction.

Alternatively, light-emitting diodes (LED's) and laser diodes can be considered for optoacoustic signal generation due to their small size, low cost, commercial availability, high repetition rate tolerance, stability and ability to operate without an external active cooling system [10–14]. LED's feature emitting areas of approximately 1×1 mm^2 and no output facet reflectivity. LED's are available in a wide range of wavelengths including the visible and the near-infrared (NIR) region. Moreover, they generally provide energies on the order of a few μJ up to a few hundred of μJ/pulse, although with a relatively long pulse width on the order of 100–500 ns. Commercially they are also available in stacks of multiple LED's in order to increase the output power. Due to their large emitting region, long pulse width and higher energy output, they are suitable only for broad-field illumination and have been used only in tomography systems such as in [12], achieving penetration depths of 15 mm and lateral resolution of ~500 μm.

Abbreviations: CNR, contrast to background ration; COD, catastrophic optical damage; CW, continuous wave; DAQ, data acquisition card; FWHM, full width at half maximum; MIP, maximum intensity projection; NIR, near-infrared; OPO, optical parametric oscillator; PLD, pulsed laser diode; SNR, signal-to-noise ratio; TTL, transistor-transistor-logic; UST, ultrasound transducer; VIS, visible.

* Corresponding author.
E-mail address: v.ntziachristos@tum.de (V. Ntziachristos).

[1] These authors contributed equally to this work.

https://doi.org/10.1016/j.pacs.2017.12.002

Pulsed laser diodes (PLD's) feature emitting areas as large as $800 \times 400\ \mu m^2$ and low output facet reflectivity [15], and they emit only within the NIR region. A PLD with energy output up to a few mJ has been reported using an expensive laser diode in a tomography set-up that has been shown to interrogate phantoms at depths up to 3 cm with 40–60 μm lateral resolution [16,17]. However, typical commercial PLD's provide pulse energies of only several μJ and are available only in the NIR [18,19], making them suboptimal for optoacoustic mesoscopy of biological tissue, since the absorption coefficient of hemoglobin is 2–3 orders of magnitude lower in the NIR range than in the visible range. The resulting low contrast in the wavelength range of 650–1200 nm makes it difficult to image blood capillaries, a limitation that can be partially compensated by prolonging the pulse duration to 100–200 ns in order to increase the pulse energy delivered [10,18–20], but this reduces spatial resolution. To solve this issue, optical resolution optoacoustic microscopy has been achieved using pulsed diodes, but only at depths considered shallow for NIR optoacoustic imaging: one set-up achieved 1.5 μm lateral resolution and 96 μm axial resolution to a depth of 80 μm [20].

In contrast to PLD's, continuous wave (CW) diodes can emit in the visible range, which could allow satisfactory SNR even when using lower pulse energies, due to the higher blood absorption in the visible over NIR. CW laser diodes feature small emitting areas to keep the driving current low and high output facet reflectivity to increase the efficiency [15]. In contrast to LED's, CW laser diodes can be focused tighter and provide shorter pulse widths, making them more suitable for high-resolution imaging. Previous studies used CW laser diodes operating in pulse mode within their nominal current limits, achieving pulse energies of several nJ but necessitating coherent signal averaging over many pulses in order to increase the SNR [21–23]. As a result, a single measurement can take between 50 milliseconds at a repetition rate of 30 kHz (1500 averages) [22] and 500 milliseconds at a repetition rate of 1 kHz (512 averages) [23]. These studies used CW laser diodes only for microscopic application where lower energies per pulse are sufficient.

In this paper, we interrogated whether we could use CW laser diodes to generate more energy output per pulse and capitalize on several of their advantages, including a broader range of available wavelengths and reduced cost. We hypothesized that overdriving CW laser diodes with ultra-short current pulses can deliver stronger light pulses than when using nominal values, without damaging the diode. Therefore, our expectation was that by better matching diode emission wavelength to the absorption maximum of hemoglobin and by overdriving the diodes, we could improve SNR and resolution for imaging applications where maximizing penetration depth is not the primary goal. We developed a laser current-driver and investigated the pulse output characteristics and the longevity of CW laser diodes emitting in the visible and NIR range under different pulsed current conditions. Using laser diode overdriving, we performed raster-scanning mesoscopy of phantoms and biological tissue *in-vivo*. We demonstrate how it is possible to achieve much faster pulse repetition rates than previously reported in optoacoustic microscopy, opening up the possibility of using small, inexpensive CW laser diodes for fast optoacoustic applications.

2. Materials and methods

2.1. Pulsed laser diode driver

A laser-diode driver was constructed (Fig. 1a) to deliver high-current, nanosecond pulses at high repetition rates. The driver design is a modified and simplified version of a driver developed for laser radar applications [24]. The working principle is as follows: the capacitor *C* is charged at high voltage *HV* through the R_c - *C* - D_1 circuit. An external Transistor-Transistor-Logic (TTL) pulse triggers the power MOSFET Q_1 (DE275-501N16A; IXYS, USA); as the power MOSFET conducts, capacitor *C* is discharged via laser diode *LD*. The capacitor *C* and the power MOSFET can operate at voltages up to 500 V. Resistor R_{CL} limits the current to the desired value. This design allows the current amplitude to be controlled through the high voltage amplitude. The rise time of the current pulse is determined by the turn-on speed of the power MOSFET, while the fall time is determined only by the time constant of the R_{CL}–*C* –*LD*–Q_1 circuit. Through this design, the pulse duration can be controlled by changing the capacitance value. Typical values of the components are: $R_C \cong 3.4\ k\Omega$, $C \cong 400\ pF$, $R_{CL} \cong 1\ \Omega$, $R_M \cong 0.1\ \Omega$. This driver can provide the combination of very low pulse width ($\sim$<10 ns), high current ($\sim$<50–60 A) and high repetition rate ($\sim$>500 kHz), which commercially available laser diode drivers do not offer [25].

2.2. Diode characterization

We tested six laser diodes emitting in the visible and NIR region (Table 1) by pulsing them with the driver presented above at 50 kHz, using a function generator (33522B; Keysight, USA) to trigger the driver. The pulse peak current was adjusted by varying the high voltage from 10 to 270 V in steps of 10 V using a variable voltage supply with maximum 300 V output (EA-3050B; EA, Germany). The optical output of each laser diode was measured using a biased photodiode (DE10A/M; Thorlabs, USA) and recorded using a digital oscilloscope (DPO 7254; Tektronix, USA). The same oscilloscope was connected to the driver's current monitor output in order to measure the peak current. Optical output measurements were averaged 1000 times, and the averages were used to determine the full-width-at-half-maximum (FWHM) optical pulse width. The mean output power was measured using a hand-held

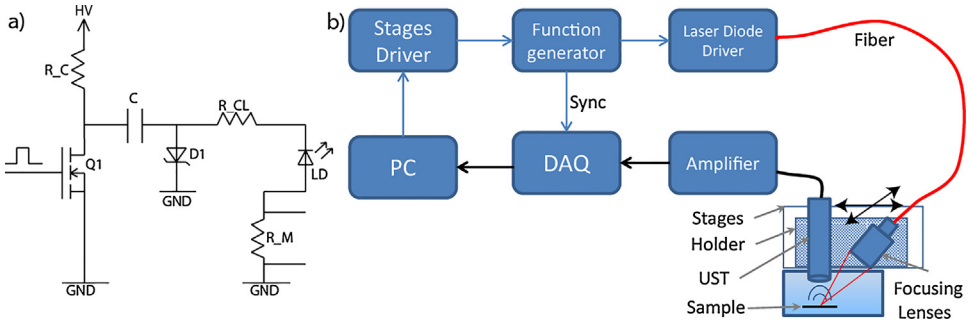

Fig. 1. **(a)** Schematic of the laser diode driver presented here. **(b)** Schematic of the laser diode-based optoacoustic imaging system. DAQ, data acquisition card; PC, personal computer; UST, ultrasound transducer.

Table 1
Characteristics of the laser diodes used with the driver. The "CW Power" and "CW Current" columns indicate the manufacturer-specified absolute maximum power and current in CW operation, respectively.

Laser Diode	Package Type (TO Can)	Wavelength (nm)	CW Power (W)	CW Current (A)	Manufacturer
NDB7K75	Ø9 mm	445	3.5	3.0	Nichia, Japan
TB450B	Ø5.6 mm	450	1.6	1.6	Osram OS, Germany
HL63193MG	Ø5.6 mm	638	0.7	1.0	Oclaro, USA
RLT780-1000G	Ø9 mm	780	1.0	1.4	Roithner LaserTechnik, Austria
L808P1000MM	Ø9 mm	808	1.0	1.5	Thorlabs, USA
RLT830-1.5G	Ø9 mm	830	1.5	2.1	Roithner LaserTechnik, Austria

laser power meter (Edmund Optics, USA). To measure the wavelength emitted by the laser diodes we used a USB Spectrometer (Ocean Optics Spectrometer 2000, Ocean Optics, USA). To test the output power stability as a function of the repetition rate we used the same function generator, photodiode and power meter as above.

2.3. Laser diode-based imaging system

To further characterize the imaging performance using CW laser diodes, we developed a raster-scanning system [26,27] for optoacoustic measurements (Fig. 1b). Matlab, installed on a PC, controls two linear stages (M-663; Physik Instrumente, Germany), which are mounted at 90° with respect to each other, forming an X-Y scanner. A custom-made, 3D-printed holder mounted on each stage contains a spherically focused, 28.8 MHz transducer with 112% bandwidth and f-number of 1.07 (SNX160333_HFM29; Sonaxis, France) as well as the lens system. Stage motion is controlled using a stage driver (C-867.260; Physik Instrumente). The x-stage moves at a constant velocity, and when it reaches the required position, the stage driver causes the function generator (33522B; Keysight, USA) to generate a train of N pulses at the required repetition rate, where N is also the number of pulses that are averaged for a given A-scan. This pulse train triggers the laser diode driver. Once a B-scan is complete, the y-stage moves the transducer to the next line and the entire process repeats.

Light from the laser diode is coupled to a multimode glass fiber with a diameter of 400 μm and numerical aperture (NA) of 0.5 (M45L01; Thorlabs). This coupling is achieved by immobilizing the fiber tip against the emitting window of the laser diode. The coupling efficiency is high (approximately 80%) because the NA and diameter of the light beam emitted by the diode are smaller than the NA and diameter of the fiber. The light pulse is focused on the sample by the lens system. The focusing lens system consists of a fiber collimator (F220SMA-532; Thorlabs) with focal length of f_1 = 10.9 mm and a focusing lens (A260-A; Thorlabs) with focal length f_2 = 15.29 mm, giving a magnification ratio (f_2/f_1) of 1.4 and an illumination spot with a diameter of ~560 μm. The generated optoacoustic signal is received from the transducer and amplified by a low-noise amplifier (AU-1291-R; Miteq, USA). The signal is then acquired by a high-speed DAQ (Razor Express 14 × 2 CompuScope; Dynamic Signals, USA), averaged N times in Matlab, and saved. Despite good shielding, we found that the current driver caused strong interference in the acquired signal, which we could separate from the signal based on the 2- to 3 μs lag between when the ultrasound signal leaves the sample and when it arrives at the transducer.

The illumination area was measured using a CCD camera (daA1920-30 um; Balser AG, Germany). The FWHM size of the illumination spot was found to be 880 μm in one direction and 720 μm in the other, forming an ellipse. This ellipse pattern is generated because the sample is illuminated at an angle of ~ 60° with respect to the imaging plane. The illumination area was estimated to be 0.63 mm^2.

2.4. Experimental measurements

To examine the use of CW laser diodes in imaging applications, we employed a suture phantom and explored the resolution achieved. The Suture Phantom consisted of three black sutures with diameters of 20, 30 and 50 μm crossing one another. The sutures were parallel to the imaging plane and immersed in clear water. Image data were obtained using a pulse repetition rate of 625 kHz; data for a field of view measuring 4 × 4 mm^2 were averaged 200 times. The raster-scan step size was 5 μm.

To examine the use of CW laser diodes for *in vivo* applications, we imaged the ear of an intact, healthy, adult CD-1 albino mouse under anaesthesia. Image data were obtained using a pulse repetition rate of 625 kHz; data for a field of view measuring 5 × 5 mm^2 were averaged 500 times. We also studied the median surface of the lower forearm of a healthy human volunteer. Image data were obtained using a pulse repetition rate of 156 kHz; data for a field of view measuring 5 × 5 mm^2 were averaged 500 times. For these two measurements, the raster-scan step size was 25 μm. All procedures with animals and humans were approved by the District Government of Upper Bavaria.

For all the imaging experiments, the TB450 B laser diode was used because we were able to couple the light only with diodes in a Ø5.6 mm package (TB450B, HL63193MG) but not the diodes in a Ø9 mm package, and because blood should absorb more strongly at the TB450 B wavelength. The applied voltage at the current driver was 300 V and the driving current ~52 A. The energy per pulse for the TB450 B was 72 nJ after the lens system, and the pulse width was ~10 ns.

Images were reconstructed using a 3D beam-forming algorithm to achieve constant lateral resolution at all depths [28]. The directivity and sensitivity field of the detectors was taken into account; each detector can detect a signal within a cone with a specific opening related to the f-number of the transducer [26]. The voxel size of the reconstructed 3D-volume was 20 × 20 × 10 μm for reconstruction of images of mouse ear and human forearm. The voxel size for the reconstruction of images from suture phantom was 20 × 20 × 5 μm.

The Contrast-to-Background Ratio (CNR) in the human arm image was computed for 14 points (volume elements) on the blood vessels reconstructed, at different depths. CNR was calculated as $CNR = 10\log(\frac{S-B}{B})$, where S is the root mean square value of the signal at each depth and B is the standard deviation of the background noise [29].

2.5. Longevity testing of the laser diodes

To test the performance of the laser diode over extended periods of times, we connected two laser diodes TB450B (Osram, Germany) and HL63193MG (Oclaro, USA) to an optical fiber (M45L01; Thorlabs, USA) to simulate the conditions of the setup shown in Fig. 1b. Light at the output of the fiber was attenuated with an absorptive Neutral Density filter (optical density of 2; NE20B-A; Thorlabs, USA) and measured with a photodiode

(DE10A/M; Thorlabs, USA). Attenuation was necessary to avoid photodiode saturation. We employed bursts of 500 pulses at a repetition rate of 625 kHz repeated every 2.4 ms to mimic the scan parameters employed in the imaging of the mouse ear *in vivo*. The applied voltage on the current driver was 300 V. The photodiode signals were recorded by a digital oscilloscope (DPO 7254; Tektronix, USA) with 2.5 GS/s sampling rate and averaged 500 times; the peak voltage and FWHM pulse width of each averaged optical pulse was saved on the PC. Measurements were run over 140 h, in many intermittent sections over a course of 2 weeks.

3. Results

3.1. Diode characterization

We drove CW laser diodes emitting in the visible and NIR range with nanosecond current pulses exceeding the manufacturer-specified maximum current [30] by up to 45 times. The pulse repetition rates obtained were as much as 21-fold faster than those previously reported in optoacoustic imaging [22].

Fig. 2 shows laser diode performance under nanosecond current pulses and a maximum driver voltage of 270 V. The maximum current applied was different for each laser diode because of differences in the internal dynamic resistance of each diode. Fig. 2a displays, for each diode, the energy per pulse, pulse width, peak power and emitted wavelength as a function of the peak current. The results show that the laser diodes provided as much as 200 nJ of energy per pulse. The pulse width for the L808P1000 M diode at 808 nm was maximal at around 20 A and showed overall non-monotonic behavior. For all diodes, the current pulse width was shorter than 8 ns, with ~3 ns rise time and ~4.5 ns fall time; the optical pulse width was shorter than 10 ns. The main limiting factor for shortening the pulse width appears to be inductance on the printed circuit board and the laser diode package, which prevents fast changes in the current. The peak power was not proportional to the energy per pulse, because pulse width varies as a function of the current that drives the laser diode. We observed a small shift of the wavelength towards shorter wavelengths by ~3 nm in pulsed operation relative to CW operation for all laser diodes. In pulsed operation, the wavelength was constant for all values of the applied current. The maximum voltage for these experiments was chosen to be 270 V to avoid permanent damage of the laser diodes, since the diodes L808P100MM and RLT780-1000G appeared to show power saturation close to this voltage. In contrast, diodes TB450B and HL63193MG showed stable operation at 300 V, the maximum voltage of the power supply.

Fig. 2b shows the maximum output power and the wavelength as a function of the repetition rate used. There was no decrease in the peak power at higher repetition rates, and the wavelength was stable. These results indicate that during pulsed operation, the laser diodes provided up to 27-fold greater optical power than the manufacturer-specified absolute maximum power in CW mode. The diodes also showed stable operation at different repetition rates.

We examined the divergence of the laser diodes when overdriven. They appeared to show greater divergence than in CW mode (data not shown). Nevertheless, this should affect only

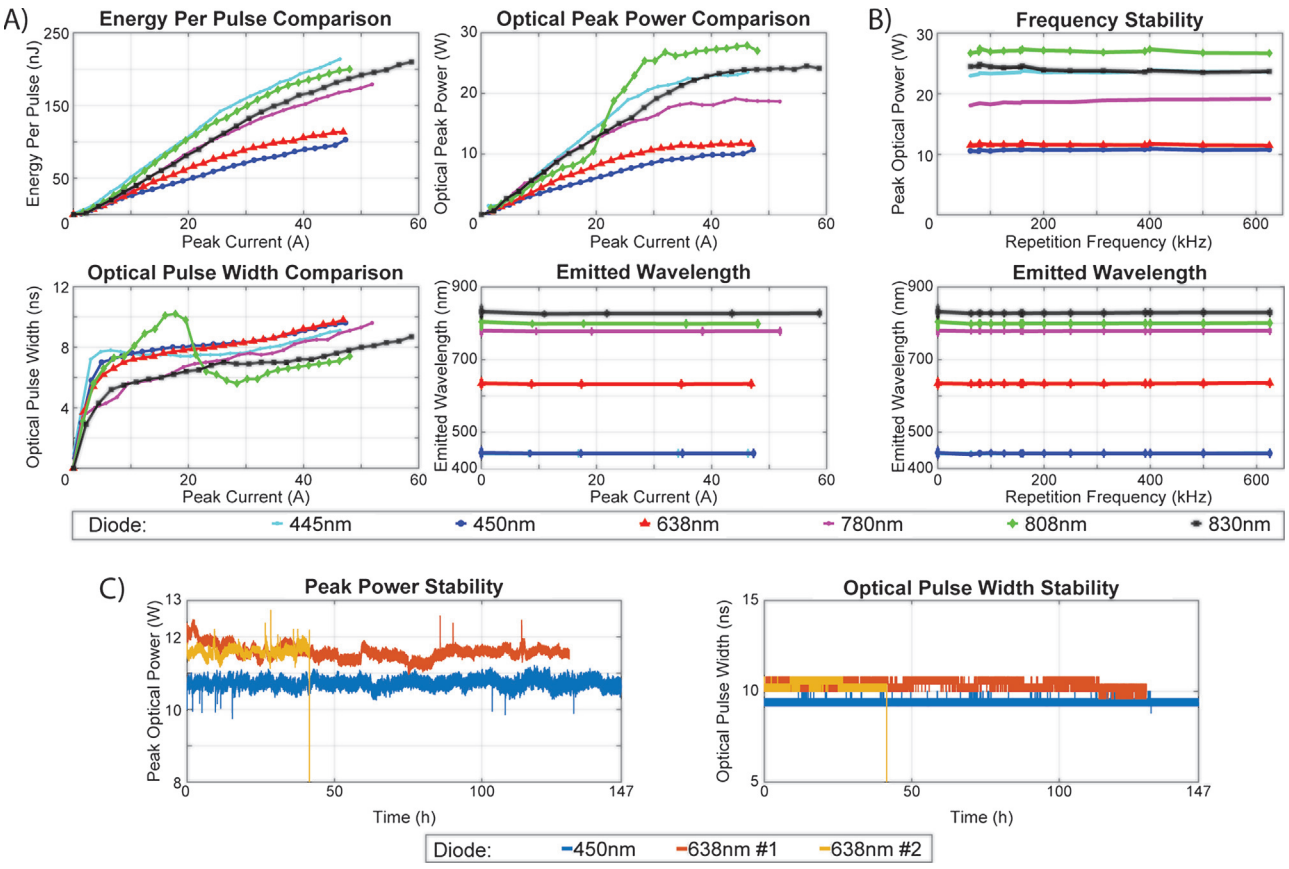

Fig. 2. Performance comparison of laser diodes emitting nanosecond pulses. (a) Energy per pulse, optical pulse width, optical peak power and wavelength vs peak current. The data for the 445-nm and 450-nm diodes in the "Emitted Wavelength" graph overlap. (b) Optical peak power and wavelength vs repetition rate. The data for the 445-nm and 450-nm diodes in the "Emitted Wavelength" graph overlap. (c) Longevity test of three laser diodes (TB450B, HL63193MG-#1 and HL63193MG-#2), showing peak power and pulse width as a function of total working hours. The wavelength emitted at CW operation is plotted at Peak Current and Repetition Frequency '0'.

the coupling efficiency of the light into the multi-mode fiber. As long as the numerical aperture of the laser diode is smaller than that of the fiber and as long as the fiber lies close enough to the diode, the coupling efficiency should remain high. All measurements shown below take into account this potential drop in coupling efficiency due to the increase in output divergence of the laser diodes.

Fig. 2c shows the peak power and the pulse width of the 3 laser diodes as a function of laser operating time. One laser diode, HL63193MG-#2, was destroyed after >40 h of operation without showing any previous sign of degradation. The other 2 laser diodes, HL63193MG-#1 and TB450B, showed no degradation in performance, peak power or pulse width, after respective operating times of ~130 and ~150 h. The standard deviation of the peak power of the light pulse was <2% for all 3 laser diodes, indicating stable laser diode efficiency over long operating times. Discontinuities in the peak power graph were observed and they corresponded exactly with the ending of one measurement and the beginning of the next one. We observed a slight increase in TB450B output power and a slight decrease in HL63193MG output power every time we turned these diodes on, until they reached thermal equilibrium. However, even after >140 h of operation, the two laser diodes did not exhibit power output deterioration; instead power output remained stable around 10 W. During these measurements, a small heat sink was installed on the driver. The metal connector also acted as a small heat sink for the laser diodes. The temperature of the driver (MOSFET and R_C) remained stable at around 60 °C, and the temperature of the laser diode remained at ambient temperature.

3.2. Maximum permissible exposure limits

According to the maximum permissible exposure limits outlined by the American National Standards Institute [31], a single laser pulse at 450 nm may have a maximum energy density of 20 mJ/cm^2 and a maximum permissible power density of 18 W/cm^2 for the duration of the measurements. Based on the experimental conditions for the *in vivo* measurements, we

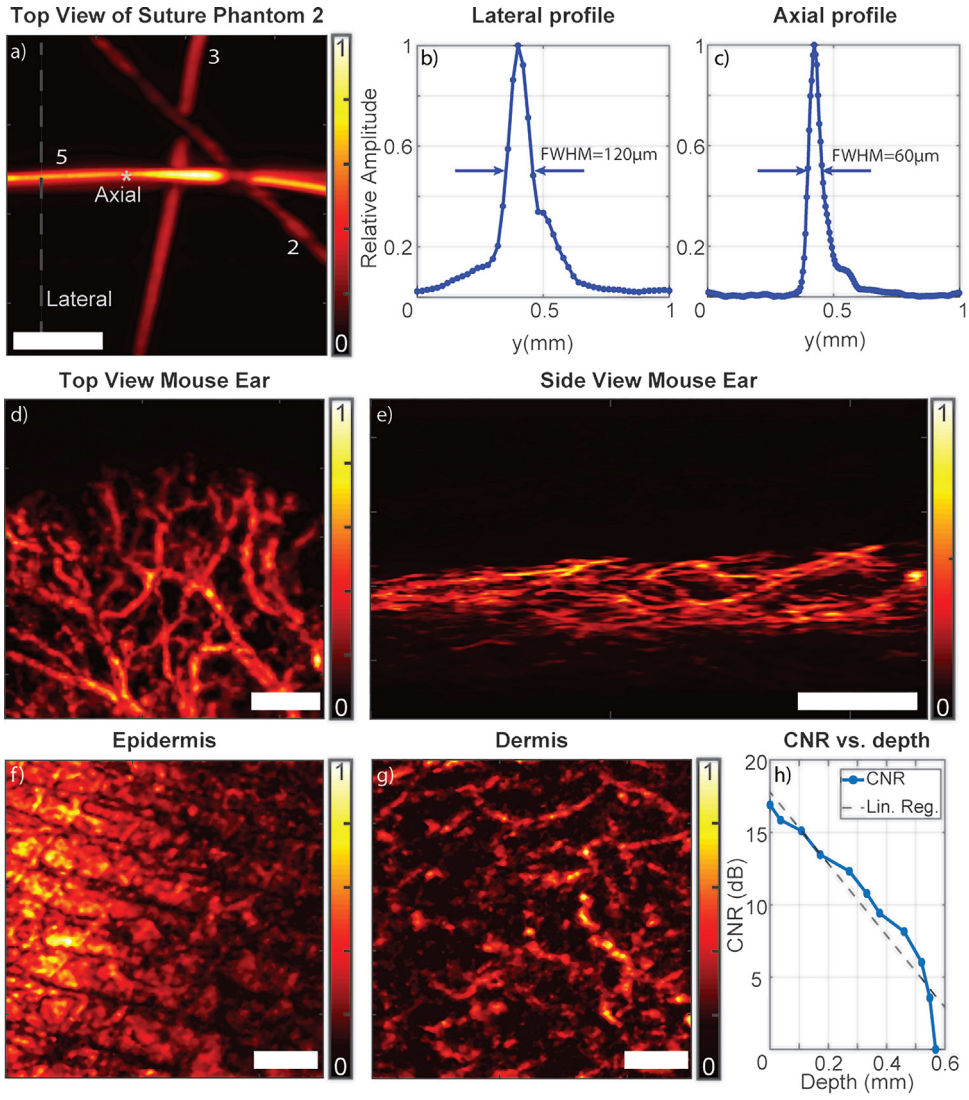

Fig. 3. Performance of the overdriven CW laser diode system for optoacoustic imaging. (a) Top view of the Suture Phantom. Suture diameters are indicated as follows: 2, 20 μm; 3, 30 μm; 5, 50 μm. (b) Profile of the lateral line shown in panel a. (c) Profile of the axial point shown in panel a. (d-e) Amplitude images of a mouse ear showing vasculature, including smaller vessels. (f-g) Coronal maximum-intensity projections of human forearm imaged at depths ranging from 0 to 280 μm (epidermis) and from 280 to 550 μm (dermis). The two skin layers show different patterns, with microvasculature evident in the dermis. (h) Contrast-to-noise ratio (CNR) as a function of penetration depth when imaging the human forearm. A best-fit line calculated by linear regression (Lin. Reg.) is shown for reference. Scale bars, 1 mm.

calculate a pulse energy density of 4.6 μJ/cm^2 and mean power density of 3.18 W/cm^2, both of which are well within maximum exposure limits.

3.3. Imaging performance

Fig. 3 presents the imaging performance of the overdriven laser diodes in phantoms as well as *in vivo*. Fig. 3a shows the top view of the reconstructed image for the Suture Phantom. Fig. 3b presents a profile of the reconstructed and Hilbert-transformed optoacoustic signal across the 50-μm suture at the lateral line shown in Fig. 3a. The FWHM of the signal was 120 μm, corresponding to a lateral resolution of 110 μm. Nevertheless, the 20 μm suture was still visible. Fig. 3c presents a profile of the reconstructed and Hilbert-transformed optoacoustic signal across the 50 μm suture at the axial point shown in Fig. 3a. The FWHM of the signal was 60 μm, corresponding to an axial resolution of 33 μm.

To test the ability of the overdriven laser diode system to image biological tissue, we imaged a mouse ear *in vivo*. We imaged a field of view of 5 × 5 mm^2 using a 25 μm step size over an acquisition time of 97 s. Fig. 3d and e show, respectively, top and side views of a mouse ear. Mouse ear vasculature was well resolved, and smaller vessels were also visible.

To test the ability of the overdriven laser diode system to image thick biological tissue, we imaged human skin *in vivo*. Fig. 3f and g shows top views of a human forearm imaged at different depths. Fig. 3f extends from the surface down to a depth of 280 μm, where epidermis is expected. Fig. 3g extends from a depth of 280 μm to a depth of 550 μm, where dermis is found. Microvasculature is visible in this deeper region. The regions corresponding to epidermis and dermis appear different in the images, suggesting that they can be differentiated using this technique.

Fig. 3h presents the CNR computation as a function of depth for voxels reconstructed from different vessels and depths. CNR was 15–20 dB for the first 100 μm, and it dropped rapidly with depth. This reflects strong absorption and scattering of blue light by tissue. Use of different wavelengths and illumination geometries may increase the penetration depth achieved.

4. Discussion

In this paper we have shown that CW laser diodes, pulsed far beyond their nominal CW current limit, can provide short, nanosecond optical pulses with energies of a few hundred nJ. Moreover, they can be pulsed with high repetition rates, up to more than 600 kHz, enabling fast, high-SNR optoacoustic imaging through averaging.

The fact that we achieved such sustained overdriving of these commercial diodes reflects the main mechanisms of laser diode damage. The first one is catastrophic optical damage (COD) [32], which occurs when photon density on the facet of the laser diode is high enough to damage the diode; in other words, a single pulse of very high power can damage or degrade the diode. Previous studies with laser diodes have shown that the maximum peak power that a laser diode can provide is inversely proportional to the square root of the pulse width, $P \propto \frac{1}{\sqrt{t}}$ [30]. Therefore, the longer the pulse width is, the smaller the maximum peak power can be provided by the laser diode before being damaged by COD. The other damage mechanism, thermal damage, occurs when the dissipated power heats up the diode beyond its destruction threshold. COD limits the maximal pulse energy, while thermal tolerance limits the maximal repetition rate. Our data suggest that commercial CW laser diodes can be operated near the tolerance limits for both kinds of damage. As long as operating conditions do not exceed either limit, these laser diodes appear to show stable performance. This is, to our knowledge, the first report of overdriving laser diodes for optoacoustic imaging.

The repetition rate can be further increased as long as the mean optical output power of the CW laser diode remains below the manufacturer-specified damage threshold. In this way, more averages can be acquired in less time, drastically reducing the imaging time. In the present work, we were able to operate the CW laser diodes with a duty cycle of 0.6%, compared to a maximum duty cycle of 0.1% for pulsed laser diodes. In addition, we were able to acquire 500 averages in only 0.8 ms, approximately 60 times faster than previously reported [22].

We succeeded in operating some laser diodes for more than 135 h (∼1 × 10^{11} pulses) under challenging conditions, *i.e.* using 10 ns pulses at a repetition rate of more than 600 kHz and peak current of about 50 A, without diode damage or degradation of optical signal. These findings demonstrate the durability and damage resistance of laser diodes when overdriven in the set-up presented. One of the laser diodes used (HL63193MG-#2) was permanently damaged after ∼40 h of operation without any previous sign of degradation. We intentionally used another diode of the same kind (HL63193MG-#1), which then operated for more than 130 h without any power deterioration. Therefore, we suspect that HL63193MG-#2 burned out because of a manufacturing defect, rather than because of intrinsic performance limits. Even after such burn-out, replacing a CW laser diode is much less expensive and simpler than repairing an OPO laser. Future experiments with stronger power supplies are needed to assess diode performance at peak power levels closer to the COD threshold.

Our goal in this study was to demonstrate good SNR and resolution with overdriven CW laser diodes in optoacoustic imaging, because this could allow much more cost-effective imaging of biological samples in the visible range of the spectrum, where hemoglobin absorbs more strongly than in the NIR region typically used in optoacoustics. CW diodes are also available in the NIR region, where other biological absorbers such as lipids and proteins absorb more strongly than in the visible range. In this way, overdriven CW laser diodes present a more flexible and substantially more cost-effective alternative to PLD's for optoacoustic imaging *in vivo*. Especially at the lower energies associated with CW diodes, a good match between the emission wavelength and absorption maximum of the target absorber is critical. Thus, we could not image vasculature in mouse ear when we used the 638 nm diode (data not shown). At the same time, PLD's operate only in the NIR region and at higher energies than CW laser diodes, allowing PLD's to penetrate deeper in tissues. Our present study justifies future work systematically comparing under what conditions and for what absorbers our relatively high SNR obtained at visible wavelengths after high averaging can outperform the SNR of higher-energy PLD's at NIR wavelengths.

Our results with overdriven CW laser diodes form part of a recent trend towards developing miniaturized, low-cost diode alternatives to conventional laser sources for optoacoustic imaging. We suspect that, as work continues on developing CW diodes, PLD's and LED's, each type of illumination source may emerge as a more cost-effective choice for specific optoacoustic applications. For example, LED's can provide long, strong pulses in the visible and the NIR, making them suitable for broad-field illumination in tomography, but with limited resolution. PLD's can provide higher resolution than LED's, but their availability only in the NIR range means that pulses lasting ∼100–200 ns are required to obtain strong signal from hemoglobin, which limits lateral resolution when imaging tissues. Overdriven CW laser diodes in the visible range can also provide higher resolution than LED's and may provide much stronger SNR than PLD's when imaging hemoglobin in tissues, but at shallower depths.

The acoustic focus employed in the present work was sharper than the optical illumination area. Therefore, the lateral resolution achieved in the images depended on the acoustic focusing of the transducer. The overall resolution of the system can be improved by using transducers with a higher central frequency or wider bandwidth, using a shorter pulse width or by focusing the light to a sharper spot than the acoustic focus, such as in optical-resolution optoacoustic microscopy applications. The axial resolution achieved in the present work was 33 μm, which is greater than the theoretical limit of 20 μm based on calculations described in [33]. The lateral resolution was 110 μm, which is greater than the theoretical limit of 82 μm based on [34]. The observed axial and lateral resolution probably result from the 60° angle of illumination, which creates uneven illumination across the sensitivity field of the transducer, which is inconsistent with the assumption of homogeneous illumination made during reconstruction [26,28]. Increasing the homogeneity of illumination may improve the lateral resolution and possibly also penetration depth.

The laser diode-based optoacoustic imaging system described here operates in epi-illumination mode, making it suitable for small, hand-held measurements and *in vivo* observations. Imaging within thin tissue (mouse ear) and thick tissue (human arm) was demonstrated and points to new possibilities for low cost, diode-based optoacoustic tissue readings. In the future, we expect to adapt the technology developed to be able to make use of diodes with Ø9 mm packaging as well as to exploit optical methods to focus the light of the laser diodes into optical fibers. Moreover, we aim to combine different wavelength diodes covering the entire visible and NIR range (445–930 nm) into the same illumination path, for enabling multispectral tissue interrogation and spectroscopy. Multispectral measurements and spectroscopy will require pulse-to-pulse monitoring of the laser power, since even small fluctuations of 2% could heavily influence spectral un-mixing methods [35].

In conclusion, we have confirmed that overdriven CW laser diodes can be used as optoacoustic light sources and they come with the advantages of low cost and size, broad wavelength availability and high repetition rates that can enable fast multispectral imaging and sensing applications in biology and the environment.

Acknowledgements

The research leading to these results was funded by the Helmholtz Association within the funding program Helmholtz Enterprise Initiating Networking Funds(HE-2014-4, DERMA-SIGHT); the Bundesministerium für Bildung und Forschung (BMBF), Bonn, Germany (Project Sense4Life, 13N13855); and the European Union's Horizon 2020 research and innovation programme under grant agreement no. 687866 (INNODERM).

We would like to thank the reviewers for their valuable comments that helped to improve the quality of this paper.

References

[1] V. Ntziachristos, D. Razansky, Molecular imaging by means of multispectral optoacoustic tomography (MSOT), Chem. Rev. 110 (5) (2010) 2783–2794.
[2] J. Yao, L.V. Wang, Sensitivity of photoacoustic microscopy, Photoacoustics 2 (2) (2014) 87–101.
[3] J. Hui, et al., Bond-selective photoacoustic imaging by converting molecular vibration into acoustic waves, Photoacoustics 4 (1) (2016) 11–21.
[4] A. Taruttis, G.M. van Dam, V. Ntziachristos, Mesoscopic and macroscopic optoacoustic imaging of cancer, Cancer Res. 75 (8) (2015) p. 1548.
[5] C. Li, L.V. Wang, Photoacoustic tomography and sensing in biomedicine, Phys. Med. Biol. 54 (19) (2009) R59–R97.
[6] L.V. Wang, Tutorial on photoacoustic microscopy and computed tomography, IEEE J. Sel. Top. Quantum Electron. 14 (1) (2008) 171–179.
[7] L.V. Wang, J. Yao, A practical guide to photoacoustic tomography in the life sciences, Nat. Methods 13 (8) (2016) 627–638.
[8] V. Ntziachristos, Going deeper than microscopy: the optical imaging frontier in biology, Nat. Methods 7 (8) (2010) 603–614.
[9] M. Schwarz, et al., Three-dimensional multispectral optoacoustic mesoscopy reveals melanin and blood oxygenation in human skin in vivo, J. Biophotonics 9 (1-2) (2016) 55–60.
[10] R.G.M. Kolkman, W. Steenbergen, T.G. van Leeuwen, In vivo photoacoustic imaging of blood vessels with a pulsed laser diode, Lasers Med. Sci. 21 (3) (2006) 134–139.
[11] P.K. Upputuri, M. Pramanik, Performance characterization of low-cost, high-speed, portable pulsed laser diode photoacoustic tomography (PLD-PAT) system, Biomed. Opt. Express 6 (10) (2015) 4118–4129.
[12] T.J. Allen, P.C. Beard, High power visible light emitting diodes as pulsed excitation sources for biomedical photoacoustics, Biomed. Opt. Express 7 (4) (2016) 1260–1270.
[13] T. Agano, et al., Comparative experiments of photoacoustic system using laser light source and LED array light source, SPIE BiOS, SPIE, 2015.
[14] X. Dai, H. Yang, H. Jiang, In vivo photoacoustic imaging of vasculature with a low-cost miniature light emitting diode excitation, Opt. Lett. 42 (7) (2017) 1456–1459.
[15] P. Rainbow, High-power pulsed laser diodes take on new industrial and commercial applications, Photonics Spectra (2004) p. 4.
[16] A. Kohl, et al., An Ultra Compact Laser Diode Source for Integration in a Handheld Point-of-care Photoacoustic Scanner, (2016) .
[17] K. Daoudi, et al., Handheld probe integrating laser diode and ultrasound transducer array for ultrasound/photoacoustic dual modality imaging, Opt. Express 22 (21) (2014) 26365–26374.
[18] U. Paul Kumar, P. Manojit, Pulsed laser diode based optoacoustic imaging of biological tissues, Biomed. Phys. Eng. Express 1 (4) (2015) 045010.
[19] T. Wang, et al., A low-cost photoacoustic microscopy system with a laser diode excitation, Biomed. Opt. Express 5 (9) (2014) 3053–3058.
[20] L.et al. Zeng, Portable optical-resolution photoacoustic microscopy with a pulsed laser diode excitation, Appl. Phys. Lett. 102 (5) (2013) 053704.
[21] P.-H. Wang, M.-L. Li, DVD Pickup Head Based Optical Resolution Photoacoustic Microscopy, (2012) .
[22] M.-L. Li, P.-H. Wang, Optical Resolution Photoacoustic Microscopy Using a Blu-ray DVD Pickup Head, (2014) .
[23] L. Zeng, et al., Label-free optical-resolution photoacoustic microscopy of superficial microvasculature using a compact visible laser diode excitation, Opt. Express 23 (24) (2015) 31026–31033.
[24] A. Kilpelä, J. Kostamovaara, Laser pulser for a time-of-flight laser radar, Rev. Sci. Instrum. 68 (6) (1997) 2253–2258.
[25] http://picolas.de/product/ldp-v-240-100-v3/. [cited 2017 03.11].
[26] M. Omar, J. Gateau, V. Ntziachristos, Raster-scan optoacoustic mesoscopy in the 25–125 MHz range, Opt. Lett. 38 (14) (2013) 2472–2474.
[27] M. Schwarz, et al., Implications of ultrasound frequency in optoacoustic mesoscopy of the skin, IEEE Trans. Med. Imaging 34 (2) (2015) 672–677.
[28] M. Omar, et al., Ultrawideband reflection-mode optoacoustic mesoscopy, Opt. Lett. 39 (13) (2014) 3911–3914.
[29] H. He, et al., Improving optoacoustic image quality via geometric pixel super-resolution approach, IEEE Trans. Med. Imaging 35 (3) (2016) 812–818.
[30] M.et al. Ziegler, Physical limits of semiconductor laser operation: a time-resolved analysis of catastrophic optical damage, Appl. Phys. Lett. 97 (2) (2010) 021110.
[31] ANSI Z136.1, – Safe Use of Lasers. 2007, Laser Institute of America, 2007.
[32] M. Bou Sanayeh, et al., The Physics of Catastrophic Optical Damage in High-power AlGaInP Laser Diodes, (2008) .
[33] J. Xia, J. Yao, L.V. Wang, Photoacoustic tomography: principles and advances, Electromagnetic waves (Cambridge, Mass.) 147 (2014) 1–22.
[34] E.W. Stein, K. Maslov, L.V. Wang, Noninvasive, in vivo imaging of the mouse brain using photoacoustic microscopy, J. Appl. Phys. 105 (10) (2009) 102027.
[35] S. Tzoumas, V. Ntziachristos, Spectral unmixing techniques for optoacoustic imaging of tissue pathophysiology, Philos. Trans. Royal Soc. A: Math. Phys. Eng. Sci. 375 (2107) (2017).

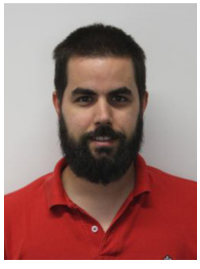

Antonios Stylogiannis holds a diploma on Applied Physics form the National Technical University of Athens (NTUA) since 2013 and a M.Sc. in Physics from Ludwig Maximilian University of Munich (LMU) since 2015. Afterwards he became a Ph.D. student at the Chair of Biological Imaging (CBI) in the Technical University of Munich (TUM) and is working in the Institute of Biological and Medical Imaging (IBMI) in Helmholtz-Zentrum-Muenchen (HMGU) under the supervision of Prof. Dr. Vasilis Ntziachristos until now. His main research focus is on developing novel small size and low cost light sources, such as laser diodes, for optoacoustic imaging and sensing applications in biology and the environment.

Ludwig Prade holds a diploma on Technical Physics from the Technische Universität München since 2013. He has been a member of the institute of biological and medical imaging (BIMI) at Technische Universität München and Helmholtz Zentrum München, Munich, Germany since 2014, were he works as a PhD student of Professor Vasilis Ntziachristos. His main research interests are optoacoustic imaging in the frequency domain, utilizing innovative light sources, such as laser diodes, to achieve label free, high speed and high resolution images.

Dr. Andreas Buehler studied Physics in the tri-national European Saar-Lor-Lux Master program of the Saarland University (Germany), the University of Nancy (France) and the University of Luxembourg (Luxembourg). After graduation he specialized in Medical Physics at the University of Heidelberg including a research stay at the Brigham and Women's Hospital in Boston (USA) where he worked on image guidance for breast irradiation setups. In 2008 he joined the Institute for Biological and Medical Imaging (IBMI) at the Helmholtz Zentrum Muenchen pursuing his PhD on multispectral optoacoustic tomography for small animal imaging. Since 2013 he leads the Clinical Optoacoustics group at IBMI. His current research activities focus on the translation of the MSOT technology to clinical applications, in particular endoscopy and cardiovascular imaging.

Dr. Juan Aguirre received his M.Sc. degree in Physics from Autonomous University of Madrid in 2007 and his M.Sc. degree in Mathematical Engineering from the Complutense University of Madrid in 2011. From 2007 to 2012 he pursued his Ph.D title in the Laboratory for Molecular Imaging of the Gregorio Maranion Hospital in Madrid, doing short stays at Foundation for Research and Technology in Greece and the University of Pennsylvania in the EEUU. After obtaining his Ph.D he joined the Institute of Biological and Medical Imaging (IBMI) at the Helmholtz Zentrum München with an individual Marie Curie Scholarship from the EU. He is currently a Junior Group Leader at IBMI. His research interests include developing and applying Optoacoustic Imaging techniques to solve unmet clinical needs.

George Sergiadis took his diploma in Electrical Engineering from the Aristotle University of Thessaloniki, Greece and his PhD from "Ecole Nationale Supérieure desTélécommunications", Paris France. Until 2015 he was with the Aristotle University of Thessaloniki, Greece, teaching Telecommunications and Biomedical Engineering, currently in leave of absence. In 2004–2005 he was a visiting researcher at Media Lab, MIT, in 2010–2011 visiting researcher in IBMI, Munich and in 2015–2016 August-Wilhelm-Scheer visiting professor in TUM, Munich, Germany. He is currently a visiting researcher in IBMI and also a Distinguished Professor at SIBET, Suzhou, China. His current research interests include medical imaging.

Professor Vasilis Ntziachristos received his PhD in electrical engineering from the University of Pennsylvania, USA, followed by a postdoctoral position at the Center for Molecular Imaging Research at Harvard Medical School. Afterwards, he became an Instructor and following an Assistant Professor and Director at the Laboratory for Bio-Optics and Molecular Imaging at Harvard University and Massachusetts General Hospital, Boston, USA. Currently, he is the Director of the Institute for Biological and Medical Imaging at the Helmholtz Zentrum in Munich, Germany, as well as a Professor of Electrical Engineering, Professor of Medicine and Chair for Biological Imaging at the Technical University Munich. His work focuses on novel innovative optical and optoacoustic imaging modalities for studying biological processes and diseases as well as the translation of these findings into the clinic.